Vietnam Journal of Science and Technology ***59*** *(5) (2021) 662-676*

doi:10.15625/2525-2518/59/5/15866

VIBRATION OF SANDWICH BEAMS REINFORCED BY CARBON NANOTUBES UNDER A MOVING LOAD

Thi Thom Tran[1, 2], Thi Hien Trinh[1], Dinh Kien Nguyen[1, 2, *]

[1]*Institute of Mechanics, VAST, 18 Hoang Quoc Viet, Cau Giay, Ha Noi, Viet Nam*

[2]*Graduate University of Science and Technology, VAST, 18 Hoang Quoc Viet, Cau, Giay, Ha Noi, Viet Nam*

[*]Email: *thomtt0101@gmail.com*

Received: 29 January 2021; Accepted for publication: 9 September 2021

Abstract. This work studies the vibration of sandwich beams reinforced with carbon nanotubes (CNTs) under moving point loads. The cores of the beams are homogeneous while their two sides are made of carbon nanotube reinforced composites. The effective properties of two face sheets are estimated through a micromechanical model. A uniform distribution (UD) and four different types of functionally graded (FG) distributions, namely FG-X, FG-Λ, FG-V, FG-O, are considered. Based on a third-order shear deformation theory, a finite element formulation is derived and used to investigate the vibration characteristics of the beams. The effects of carbon nanotube volume fraction, carbon nanotube distribution pattern and moving load velocity on beam vibration behavior are investigated and highlighted. The influence of layer thickness and span-to-height ratio on beam vibration is also examined and discussed.

Keywords: Sandwich beam; carbon nanotube reinforcement, third-order shear deformation theory; moving load; vibration analysis.

Classification numbers: 2.9.4, 5.4.2, 5.4.5.

1. INTRODUCTION

Carbon nanotubes (CNTs) with high strength, high stiffness, high aspect ratio and low density are excellent reinforcement for composite materials. The analysis of functionally graded carbon nanotube-reinforced composite (FG-CNTRC) beams has drawn considerable attention from researchers in recent years. Ke *et al.* [1, 2] investigated the nonlinear free vibration and dynamic stability of FG nano beams reinforced by single-walled carbon nanotubes (SWCNTs) using Timoshenko theory. Their results show that an increase in CNT volume fraction leads to higher natural frequencies for both uniformly distributed CNT (UD-CNT) and FG-CNTRC beams. Yas and Heshmati [3] studied free and forced vibrations of an FG nanocomposite beam reinforced by randomly straight SWCNTs under a moving load. Free vibration and buckling analysis of FG-CNTRC Timoshenko beams resting on an elastic foundation are also described by Yas and Samadi [4]. Shen and Xiang [5] presented the nonlinear bending and the thermal

postbuckling analyses of CNTRC beams. The obtained results show that the CNT volume fraction has a significant influence on the load-deflection curves of the beam. Based on Timoshenko beam theory, Ansari *et al.* [6] studied forced vibration of nanocomposite beams reinforced by SWCNTs. The third-order shear deformation theory was adopted by Lin and Xiang [7] in determining vibration frequencies of UD- and FG-CNTRC beams with various boundary conditions. Nejati and Eslampanah [8] employed the two dimensional (2D) elasticity theory to obtain buckling loads and natural frequencies of cantilever FG-CNTRC beams under axial load. Based on the first-order shear deformation beam theory and von Kármán nonlinearity, Wu *et al.* [9] investigated nonlinear vibration of imperfect shear deformable FG-CNTRC beams. Nonlinear free vibration and post-buckling of FG-CNTRC beams resting on nonlinear foundation were studied by Shafiei and Setoodeh [10]. Recently, Mohseni and Shakouri [11] investigated the free vibration and buckling of FG-CNTRC beams with variable thickness resting on elastic foundations.

Using FG-CNTRCs as facing composition in sandwich constructions to increase strength and stiffness, Wu and Kitipornchai [12] investigated free vibration and elastic buckling of sandwich beams with FG-CNTRC face sheets, giving a detail on the effects of CNT volume fraction, core-to-face sheet thickness ratio, slenderness ratio, and end supports on the free vibration and buckling behavior of sandwich beams. Ebrahimi and Farzamand Nia [13] proposed a higher-order shear deformation beam theory for free vibration analysis of FG-CNTRC sandwich beams in thermal environment. The effects of carbon nanotube volume fractions, slenderness ratio and core-to-face sheet thickness ratio on the vibration of the sandwich beams have been examined.

The influence of material gradation on the vibration of beams carrying a moving load has been investigated in recent years [14, 15]. It has been shown that the variation of material properties in spatial directions has a significant influence on both free and forced vibrations of the beams. This topic is further explored in the present work by studying vibration of FG sandwich beams reinforced by CNTs. The core of the sandwich beams is homogeneous while its two face sheets are a FG-CNT reinforced material. The effective properties of the two face sheets are determined by an extended rule of mixture. Five types of CNT distribution, namely UD, FG-X, FG-Λ, FG-V, FG-O, are considered. A third-order shear deformation finite element formulation is derived and employed to compute natural frequencies and investigate dynamic response of the beams. A parametric study is carried out to highlight the effects of carbon nanotube volume fraction, the type of carbon nanotube distribution, the beam geometry and moving load velocity on dynamic behavior of the sandwich beams.

2. FG-CNTRC SANDWICH BEAM

Figure 1 shows a sandwich beam with FG-CNTRC face sheets subjected to a concentrated load F_0, moving from the left end to the right end of the beam at a constant speed *v*. In the figure, the Cartesian coordinate system (*x*,*z*) is chosen such that the *x*-axis lies on the beam mid-plane. The beam consists of three layers, a homogeneous core and two face sheets of CNTRC material. Denoting $h_0 = -\frac{h}{2}$, h_1, h_2, $h_3 = \frac{h}{2}$ are the vertical coordinates of the bottom surface, two interfaces between the layers, and the top surface. Five types of distribution of CNTs in the beam cross-section, as shown in Figure 2 and given in Table 1, namely the UD, FG-X, FG-Λ, FG-V, FG-O, are considered.

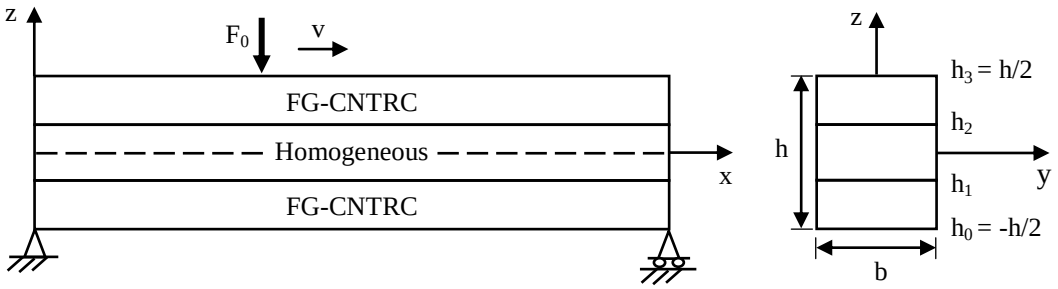

Figure 1. Geometry and coordinate system of FG-CNTRC sandwich beams under moving load

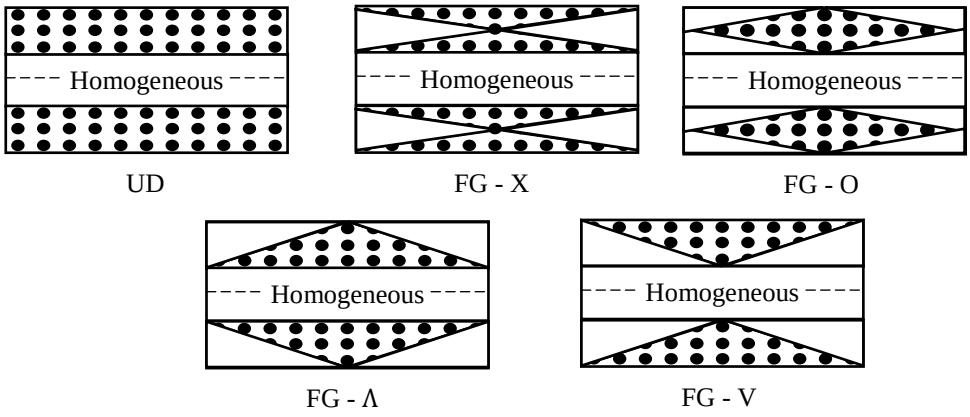

Figure 2. Cross-section of sandwich beam with five types of CNT distribution

Table 1. Volume fraction V_{CNT} of CNTs in face sheets of sandwich beam

Distribution type	Bottom face sheet $(h_0 \le z \le h_1)$	Top face sheet $(h_2 \le z \le h_3)$
UD	V_{CNT}^*	V_{CNT}^*
FG-X	$2\dfrac{\lvert h_0+h_1-2z\rvert}{h_1-h_0}V_{CNT}^*$	$2\dfrac{\lvert h_2+h_3-2z\rvert}{h_3-h_2}V_{CNT}^*$
FG-Λ	$2\dfrac{z-h_0}{h_1-h_0}V_{CNT}^*$	$2\dfrac{h_3-z}{h_3-h_2}V_{CNT}^*$
FG-V	$2\dfrac{h_1-z}{h_1-h_0}V_{CNT}^*$	$2\dfrac{z-h_2}{h_3-h_2}V_{CNT}^*$
FG-O	$2\left(1-\dfrac{\lvert 2z-h_0-h_1\rvert}{h_1-h_0}\right)V_{CNT}^*$	$2\left(1-\dfrac{\lvert 2z-h_2-h_3\rvert}{h_3-h_2}\right)V_{CNT}^*$

In Table 1, V_{CNT}^* is the total CNT volume fraction in face sheets and it is the same for the five types of the CNT distribution; V_{CNT}^* defined by $V_{CNT}^* = \dfrac{w_{CN}}{w_{CN}+\left(\rho^{CNT}/\rho^m\right)-\left(\rho^{CNT}/\rho^m\right)w_{CN}}$,

where w_{CN} is the mass fraction of nanotube, ρ^{CNT} and ρ^{m} are the densities of carbon nanotube and matrix, respectively.

The material properties of CNTRC layers are determined according to an extended rule of mixture as [12]

$$E_{11} = \eta_1 V_{CNT} E_{11}^{CNT} + V_m E^m;\ \frac{\eta_2}{E_{22}} = \frac{V_{CNT}}{E_{22}^{CNT}} + \frac{V_m}{E^m};\ \frac{\eta_3}{G_{12}} = \frac{V_{CNT}}{G_{12}^{CNT}} + \frac{V_m}{G^m} \tag{1}$$

In Eq. (1), E_{11}^{CNT}, E_{22}^{CNT} and G_{12}^{CNT} are Young's moduli and shear modulus, respectively, of the CNT; E^m, G^m and $V_m = 1 - V_{CNT}$ are Young's modulus, shear modulus and volume fraction of matrix phase, respectively; η_1, η_2, η_3 are the CNT efficiency parameters.

The Poisson's ratio of the FG-CNTRC face sheets are determined as

$$\nu_{12} = V_{CNT}\nu_{12}^{CNT} + V_m\nu^m;\quad \nu_{21} = \frac{\nu_{12}}{E_{11}} E_{22}; \tag{2}$$

where ν_{12}^{CNT}, ν^m are Poisson's ratio of the CNT and matrix, respectively.

The effective elastic and shear moduli of the *k*th layer are calculated as follows [12]

$$\begin{aligned} &E^{(k)}(z) = \frac{E_{11}}{1-\nu_{12}\nu_{21}};\ G^{(k)}(z) = G_{12}\ \ (k = 1,3) \\ &E^{(2)} = E^c;\ G^{(2)} = G^c \end{aligned} \tag{3}$$

in which E^c, G^c are the elastic and shear moduli of the core material. The effective mass density of the *k*th layer is defined as

$$\rho^{(k)}(z) = V_{CNT}\rho^{CNT} + V_m\rho^m\quad (k = 1,3);\ \rho^{(2)} = \rho^c \tag{4}$$

where ρ^c is mass density of the core material.

3. MATHEMATICAL FORMULATION

The Shi's third-order shear deformation theory [16] is adopted herewith to formulate the governing equations for the beam. This theory is derived from an elasticity formulation, rather than displacement hypothesis, which gives better results than the first-order and other simple higher order shear deformation theories. The displacements of a point in the beam in the *x* and *z* directions, $u(x,z,t)$ and $w(x,z,t)$, respectively, are given by

$$u(x,z,t) = u_0(x,t) + \frac{z}{4}(5\theta + w_{0,x}) - \frac{5z^3}{3h^2}(\theta + w_{0,x});\ \ w(x,z,t) = w_0(x,t) \tag{5}$$

where $u_0(x,t)$ and $w_0(x,t)$ are, respectively, the displacements in the *x* and *z* directions of a point on the *x*-axis; θ is the cross-sectional rotation, and *t* is the time variable. In Eq. (5) and hereafter, the subscript comma is used to indicate the derivative with respect to the variable that follows.

By using the transverse shear rotation γ_0, defined as $\gamma_0 = \theta + w_{0,x}$ [17], the axial and transverse displacements in Eq. (5) can be rewritten as follows

$$u(x,z,t)=u_0(x,t)+z\left(\frac{5}{4}\gamma_0-w_{0,x}\right)-\frac{5z^3}{3h^2}\gamma_0;\quad w(x,z,t)=w_0(x,t) \tag{6}$$

Eq. (6) gives the axial strain ε_{xx} and shear strains γ_{xz} in the forms

$$\varepsilon_{xx}=u_{0,x}+z\left(\frac{5}{4}\gamma_{0,x}-w_{0,xx}\right)-\frac{5z^3}{3h^2}\gamma_{0,x};\quad \gamma_{xz}=5\left(\frac{1}{4}-\frac{1}{h^2}z^2\right)\gamma_0 \tag{7}$$

The normal and shear stresses are given by linear elastic constitutive law as

$$\sigma_{xx}^{(k)}=E^{(k)}(z)\varepsilon_{xx};\ \tau_{xz}^{(k)}=G^{(k)}(z)\gamma_{xz}\qquad (k=1,2,3) \tag{8}$$

Using Eqs. (7) and (8) one can write the strain energy in the form

$$\begin{aligned}U&=\frac{1}{2}\int_0^L\int_A(\sigma_{xx}\varepsilon_{xx}+\tau_{xz}\gamma_{xz})\,dA\,dx\\&=\frac{1}{2}\int_0^L\Bigg[A_{11}u_{0,x}^2+2A_{12}u_{0,x}\left(\frac{5}{4}\gamma_{0,x}-w_{0,xx}\right)+A_{22}\left(\frac{5}{4}\gamma_{0,x}-w_{0,xx}\right)^2-\frac{10}{3h^2}A_{34}u_{0,x}\gamma_{0,x}\\&\quad-\frac{10}{3h^2}A_{44}\gamma_{0,x}\left(\frac{5}{4}\gamma_{0,x}-w_{0,xx}\right)+\frac{25}{9h^4}A_{66}\gamma_{0,x}^2+25\left(\frac{1}{16}B_{11}-\frac{1}{2h^2}B_{22}+\frac{1}{h^4}B_{44}\right)\gamma_0^2\Bigg]dx\end{aligned} \tag{9}$$

where $A = bh$ is the cross-section area; $A_{11},A_{12},\ldots A_{66}$ and B_{11},B_{22},B_{44} are the beam rigidities, defined as

$$\begin{aligned}\left(A_{11},A_{12},A_{22},A_{34},A_{44},A_{66}\right)&=b\int_{h_0}^{h_3}E(z)\left(1,z,z^2,z^3,z^4,z^6\right)dz\\&=b\sum_{k=1}^{3}\int_{h_{k-1}}^{h_k}E^{(k)}(z)\left(1,z,z^2,z^3,z^4,z^6\right)dz;\end{aligned} \tag{10}$$

$$\left(B_{11},B_{22},B_{44}\right)=b\int_{-h/2}^{h/2}G(z)\left(1,z^2,z^4\right)dz=b\sum_{k=1}^{3}\int_{h_{k-1}}^{h_k}G^{(k)}(z)\left(1,z^2,z^4\right)dz$$

The kinetic energy of the beam resulted from Eq. (5) has the form

$$\begin{aligned}T&=\frac{1}{2}\int_0^L\int_A\rho^{\mathrm{ef}}(z)\left(\dot{u}^2+\dot{w}^2\right)dA\,dx\\&=\frac{1}{2}\int_0^L\Bigg[I_{11}\left(\dot{u}_0^2+\dot{w}_0^2\right)+2I_{12}\dot{u}_0\left(\frac{5}{4}\dot{\gamma}_0-\dot{w}_{0,x}\right)+I_{22}\left(\frac{5}{4}\dot{\gamma}_0-\dot{w}_{0,x}\right)^2\\&\quad-\frac{10}{3h^2}I_{34}\dot{u}_0\dot{\gamma}_0-\frac{10}{3h^2}I_{44}\dot{\gamma}_0\left(\frac{5}{4}\dot{\gamma}_0-\dot{w}_{0,x}\right)+\frac{25}{9h^4}I_{66}\dot{\gamma}_0^2\Bigg]dx\end{aligned} \tag{11}$$

where the over dot denotes the derivative with respect to time variable; $I_{11},I_{12},\ldots I_{66}$ are the mass moments, defined as

$$\begin{aligned}\left(I_{11},I_{12},I_{22},I_{34},I_{44},I_{66}\right)&=b\int_{h_0}^{h_3}\rho(z)\left(1,z,z^2,z^3,z^4,z^6\right)dz\\&=b\sum_{k=1}^{3}\int_{h_{k-1}}^{h_k}\rho^{(k)}(z)\left(1,z,z^2,z^3,z^4,z^6\right)dz\quad(\mathrm{k}=1,2,3)\end{aligned}\tag{12}$$

The potential of the moving load (V) is simply given by

$$V=-\int_0^L F_0 w_0\left(x,t\right)\delta\left(x-vt\right)dx\tag{13}$$

where $\delta(.)$ is the Dirac delta function, and x is the abscissa, measured from the left end of the beam.

4. FG-CNTRC SANDWICH BEAM ELEMENT

Consider a two-node beam element with length l. The element vector of nodal displacements (**d**) contains eight components as

$$\mathbf{d}=\left\{\mathbf{d}_u\ \mathbf{d}_w\ \mathbf{d}_\gamma\right\}^T\tag{14}$$

where

$$\mathbf{d}_u=\left\{u_{01}\ u_{02}\right\}^T;\ \mathbf{d}_w=\left\{w_{01}\ w_{0x1}\ w_{02}\ w_{0x2}\right\}^T;\ \mathbf{d}_\gamma=\left\{\gamma_{01}\ \gamma_{02}\right\}^T\tag{15}$$

are, respectively, the vectors of values for u_0, w_0 and γ_0 at nodes 1 and 2. In the above equations and hereafter, a superscript 'T' denotes the transpose of a vector or a matrix.

Linear functions are used to interpolate the axial displacement u_0 and transverse shear rotation γ_0, while cubic Hermite polynomials are used for the transverse displacement w_0 as

$$u_0=\mathbf{N}\mathbf{d}_u\ ;\ w_0=\mathbf{H}\mathbf{d}_w\ ;\ \gamma_0=\mathbf{N}\mathbf{d}\gamma\tag{16}$$

where $\mathbf{N}=\left\{N_1\ N_2\right\}$ and $\mathbf{H}=\left\{H_1\ H_2\ H_3\ H_4\right\}$ are the matrices of the linear and Hermite shape functions.

Using the above interpolations, one can write the strain energy in Eq. (9) in the form

$$U=\frac{1}{2}\sum^{ne}\mathbf{d}^T\mathbf{k}\,\mathbf{d}\ \text{ with }\mathbf{k}=\mathbf{k}_{uu}+\mathbf{k}_{uw}+\mathbf{k}_{u\gamma}+\mathbf{k}_{ww}+\mathbf{k}_{w\gamma}+\mathbf{k}_{\gamma\gamma}\tag{17}$$

where *ne* is the total number of elements, and **k** is the element stiffness matrix.

In the above equation, $\mathbf{k}_{uu},\mathbf{k}_{uw},...,\mathbf{k}_{\gamma\gamma}$ are the element stiffness matrices stemming from the axial, bending, shear deformations and their couplings with the following expressions

$$\mathbf{k}_{uu}=\int_0^l \mathbf{N}_{,x}^T A_{11}\mathbf{N}_{,x}\,dx;\ \mathbf{k}_{uw}=-\int_0^l \mathbf{N}_{,x}^T A_{12}\mathbf{H}_{,xx}\,dx;\ \mathbf{k}_{u\gamma}=5\int_0^l\left(\frac{1}{4}\mathbf{N}_{,x}^T A_{12}\mathbf{N}_{,x}-\frac{1}{3h^2}\int_0^l \mathbf{N}_{,x}^T A_{34}\mathbf{N}_{,x}\right)dx;$$

$$\mathbf{k}_{ww}=\int_0^l \mathbf{H}_{,xx}^T A_{22}\mathbf{H}_{,xx}\,dx;\ \mathbf{k}_{w\gamma}=5\int_0^l\left(-\frac{1}{4}\mathbf{H}_{,xx}^T A_{22}\mathbf{N}_{,x}+\frac{1}{3h^2}\mathbf{H}_{,xx}^T A_{44}\mathbf{N}_{,x}\right)dx; \tag{18}$$

$$\mathbf{k}_{\gamma\gamma}=25\int_0^l\left[\frac{1}{16}\mathbf{N}_{,x}^T A_{22}\mathbf{N}_{,x}-\frac{1}{12h^2}\mathbf{N}_{,x}^T A_{44}\mathbf{N}_{,x}+\frac{1}{9h^4}\mathbf{N}_{,x}^T A_{66}\mathbf{N}_{,x}+\mathbf{N}^T\left(\frac{1}{16}B_{11}-\frac{1}{2h^2}B_{22}+\frac{1}{h^4}B_{44}\right)\mathbf{N}\right]dx$$

Similarly, the kinetic energy of the beam in Eq. (11) can be rewritten as

$$T=\frac{1}{2}\sum^{ne}\dot{\mathbf{d}}^T\mathbf{m}\dot{\mathbf{d}}\ \text{ with }\ \mathbf{m}=\mathbf{m}_{uu}+\mathbf{m}_{uw}+\mathbf{m}_{u\gamma}+\mathbf{m}_{ww}+\mathbf{m}_{w\gamma}+\mathbf{m}_{\gamma\gamma} \tag{19}$$

where **m** is the element mass matrix.

The expressions for the sub-matrices in the above equation are as follows

$$\mathbf{m}_{uu}=\int_0^l \mathbf{N}^T I_{11}\mathbf{N}\,dx;\ \mathbf{m}_{uw}=-\int_0^l \mathbf{N}^T I_{12}\mathbf{H}_{,x}\,dx;\ \mathbf{m}_{u\gamma}=5\int_0^l\left(\frac{1}{4}\mathbf{N}^T I_{12}\mathbf{N}-\frac{1}{3h^2}\mathbf{N}^T I_{34}\mathbf{N}\right)dx;$$

$$\mathbf{m}_{ww}=\int_0^l\left(\mathbf{H}^T I_{11}\mathbf{H}+\mathbf{H}_{,x}^T I_{22}\mathbf{H}_{,x}\right)dx;\ \mathbf{m}_{w\gamma}=5\int_0^l\left(-\frac{1}{4}\mathbf{H}_{,x}^T I_{22}\mathbf{N}+\frac{1}{3h^2}\mathbf{H}_{,x}^T I_{44}\mathbf{N}\right)dx; \tag{20}$$

$$\mathbf{m}_{\gamma\gamma}=25\int_0^l \mathbf{N}^T\left(\frac{1}{16}I_{22}-\frac{1}{2h^2}I_{44}+\frac{1}{h^4}I_{66}\right)\mathbf{N}dx$$

The discrete equation of motion for the dynamic analysis of the beam can be written in the form

$$\mathbf{M}\ddot{\mathbf{D}}+\mathbf{K}\mathbf{D}=\mathbf{F}^{\text{ex}} \tag{21}$$

where **M** and **K** are, respectively, the global mass and stiffness matrices, obtained by assembling the matrices **m** and **k** over the elements; **D** and $\ddot{\mathbf{D}}$ are, respectively, the vectors of nodal displacements and accelerations; $\mathbf{F}^{\text{ex}}$ is the vector of the nodal external force with the following form:

$$\mathbf{F}^{\text{ex}}=\sum^{ne}\mathbf{f}^{\text{ex}}, \tag{22}$$

where $\mathbf{f}^{\text{ex}}=\{0\ \ 0\ \ F_0H_1\ \ F_0H_2\ \ F_0H_3\ \ F_0H_4\ \ 0\ \ 0\}^T$ is the element nodal force vector. Except for the element under the load F_0, the element nodal force vector $\mathbf{f}^{\text{ex}}$ is zero for all other elements, and the interpolation functions $H_i\,(i=1,...,4)$ are evaluated at the current position of the force F_0. The system of Eq. (21) can be solved by the Newmark method. The average acceleration method which ensures the numerically unconditional stability is adopted herein.

5. NUMERICAL RESULTS AND DISCUSSION

A FG-CNTRC sandwich beam with simply supported ends is considered in the numerical investigation in this section. Poly-methyl methacrylate (PMMA) with material properties as $E^m=2.5\text{GPa}$, $\rho^m=1190\ \text{kg/m}^3$, $\nu^m=0.3$ is chosen for the matrix phase; the armchair (10,10) SWCNTs with

$E_{11}^{CNT}=5.6466\,\text{TPa}$, $E_{22}^{CNT}=7.08\,\text{TPa}$, $G_{12}^{CNT}=1.9445\,\text{TPa}$, $\rho^{CNT}=1400\,\text{kg/m}^3$, and $\nu^{CNT}=0.175$ are selected as reinforcements. The CNT efficiency parameters η_i are determined by matching Young's moduli E_{11},E_{22} and shear modulus G_{12} of CNTRCs obtained from the rule of mixture given by Han and Elliott [18]. For example $(\eta_1,\eta_2,\eta_3)=(0.137,1.022,0.715)$ for $V_{CNT}^{*}=0.12$; $(\eta_1,\eta_2,\eta_3)=(0.142,1.626,1.138)$ for $V_{CNT}^{*}=0.17$; $(\eta_1,\eta_2,\eta_3)=(0.141,1.585,1.109)$ for $V_{CNT}^{*}=0.28$. Titanium alloy (Ti-6Al-4V) with $E^c=113.8\,\text{GPa}$, $\rho^c=4430\ \text{kg/m}^3$, $\nu^c=0.342$ is chosen as the core material of the sandwich beam. The total thickness of the sandwich beam is 0.01 m. The ratio of homogeneous core thickness to face sheet thickness is defined by h_c/h_f. The fundamental frequency parameter is defined as

$$\mu=\omega L\sqrt{I_{110}/A_{110}}, \tag{23}$$

where A_{110} and I_{110} are the values of A_{11} and I_{11} of a homogeneous beam made from pure core material, and ω is the fundamental frequency. A uniform increment time step $\Delta t=\Delta T/200$ with ΔT as the total time necessary for the load crossing the beam, is used for the Newmark procedure. For the convenience of discussion, the following dynamic magnification factor D_d is introduced

$$D_d=\max\left(\frac{w(L/2,t)}{w_{st}}\right), \tag{24}$$

where $w_{st}=L^3F_0/48E^cI$ is the static deflection of a pure Ti-6Al-4V beam under the load $F_0=100$ kN, acting at the mid-span.

5.1. Formulation verification

Before investigating the vibration characteristics of the beam, the accuracy of the finite element model is firstly confirmed.

Table 2. Comparison of frequency parameter of sandwich beams with $h_c/h_f=8$, L/h=20

Distribution	Source	$V_{CNT}^{*}=0.12$	$V_{CNT}^{*}=0.17$	$V_{CNT}^{*}=0.28$
FG-V	Wu and Kitipornchai [12]	0.1453	0.1588	0.1825
	Present	0.1406	0.1545	0.1790
UD	Wu and Kitipornchai [12]	0.1432	0.1560	0.1785
	Present	0.1384	0.1517	0.1749

Table 3. Comparison of frequency parameter of sandwich beams with L/h=20, $V_{CNT}^{*}=0.17$

Distribution	Source	$h_c/h_f=8$	$h_c/h_f=6$	$h_c/h_f=4$
FG-V	Wu and Kitipornchai [12]	0.1588	0.1642	0.1743
	Present	0.1545	0.1608	0.1720
UD	Wu and Kitipornchai [12]	0.1560	0.1599	0.1668
	Present	0.1517	0.1563	0.1643

Table 4. Comparison of frequency parameter of sandwich beams with $V_{CNT}^{*}=0.17$, $h_c/h_f=8$

Distribution	Source	*L/h*=10	*L/h*=20	*L/h*=30
FG-V	Wu and Kitipornchai [12]	0.3124	0.1588	0.1062
	Present	0.3119	0.1580	0.1056
UD	Wu and Kitipornchai [12]	0.3070	0.1560	0.1043
	Present	0.2995	0.1517	0.1014

Tables 2-4 compare the fundamental frequency parameter of the FG-CNTRC sandwich beam with the results of Wu and Kitipornchai [12], where the differential quadrature method has been employed. The frequency parameter is received for sandwich beam with two types of CNT distribution named as FG-V and UD. Very good agreement between the frequency parameter of the present work with that reported in [12] is obtained from Tables 2-4, regardless of the total CNT volume fraction V_{CNT}^{*}, ratio h_c/h_f and aspect ratio *L/h*, noting that a Timoshenko beam theory is used to formulate governing equations in [12].

5.2. Natural frequencies

Table 5 lists fundamental frequency parameter of FG-CNTRC sandwich beam for five different types of CNT distribution. As seen from the Table, the frequency parameter μ increases with increasing the total CNTs volume fraction V_{CNT}^{*}, especially μ more significantly increases for a smaller h_c/h_f ratio.

Table 5. The fundamental frequency parameter of sandwich beam for different h_c/h_f and *L/h* ratios

L/h	Type	$h_c/h_f=8$			$h_c/h_f=6$			$h_c/h_f=4$		
		V_{CNT}^{*}			V_{CNT}^{*}			V_{CNT}^{*}		
		0.12	0.17	0.28	0.12	0.17	0.28	0.12	0.17	0.28
30	UD	0.0924	0.1013	0.1169	0.0937	0.1045	0.1230	0.0963	0.1098	0.1326
	FG-X	0.0925	0.1014	0.1170	0.0938	0.1046	0.1231	0.0965	0.1101	0.1329
	FG-O	0.0924	0.1013	0.1169	0.0936	0.1044	0.1228	0.0961	0.1096	0.1322
	FG-V	0.0939	0.1033	0.1197	0.0960	0.1074	0.1271	0.1003	0.1150	0.1395
	FG-Λ	0.0910	0.0993	0.1045	0.0914	0.1014	0.1187	0.0921	0.1045	0.1253
20	UD	0.1384	0.1516	0.1749	0.1403	0.1563	0.1838	0.1441	0.1643	0.1982
	FG-X	0.1384	0.1517	0.1750	0.1404	0.1565	0.1841	0.1444	0.1647	0.1987
	FG-O	0.1383	0.1515	0.1748	0.1402	0.1561	0.1836	0.1438	0.1639	0.1976
	FG-V	0.1406	0.1545	0.1790	0.1437	0.1608	0.1900	0.1501	0.1720	0.2085
	FG-Λ	0.1362	0.1487	0.1707	0.1368	0.1517	0.1775	0.1379	0.1517	0.1873
10	UD	0.2736	0.2994	0.3443	0.2774	0.3085	0.3616	0.2850	0.3242	0.3891
	FG-X	0.2737	0.2995	0.3445	0.2777	0.3089	0.3621	0.2856	0.3250	0.3903
	FG-O	0.2735	0.2992	0.3440	0.2771	0.3082	0.3611	0.2844	0.3234	0.3880
	FG-V	0.2779	0.3051	0.3523	0.2841	0.3173	0.3736	0.2968	0.3392	0.4091
	FG-Λ	0.2692	0.2935	0.3360	0.2705	0.2995	0.3492	0.2727	0.3084	0.3680
5	UD	0.5243	0.5708	0.6500	0.5318	0.5878	0.6806	0.5465	0.6165	0.7282
	FG-X	0.5246	0.5712	0.6506	0.5324	0.5886	0.6818	0.5478	0.6183	0.7308
	FG-O	0.5240	0.5704	0.6495	0.5313	0.5871	0.6795	0.5451	0.6146	0.7256

	FG-V	0.5325	0.5816	0.6650	0.5445	0.6042	0.7027	0.5686	0.6442	0.7640
	FG-Λ	0.5160	0.5597	0.6347	0.5188	0.5709	0.6577	0.5233	0.5871	0.6899

Of the five types of the CNT distribution, the FG-V sandwich beam has the highest frequency, while the FG-Λ sandwich beam gives the smallest result. It is easy to see that the results obtained for beam with UD, FG-X, FG-O distributions are very close together. Moreover, the decrease of the ratio h_c/h_f leads to the increase in the frequency parameter, especially at smaller values of the aspect ratio *L/h*. This is because the sandwich beam gets higher stiffness corresponding to a smaller ratio h_c/h_f. Besides, the influence of the aspect ratio *L/h* on the frequency parameter μ is also seen in the Table 5, where the frequency parameter increases with decreasing aspect ratio *L/h*.

5.3. Forced vibration

Figure 3 shows the time histories for dimensionless mid-span deflection of the sandwich beam for three types of CNT distribution, namely FG-V, UD and FG-Λ. The figure is plotted with an aspect ratio $L/h = 20$, a total CNTs volume fraction $V_{CNT}^{*} = 0.17$, two values of the ratio $h_c/h_f = 4$, $h_c/h_f = 8$ and two values of the moving load velocity, *v* = 20 m/s, *v* = 100 m/s.

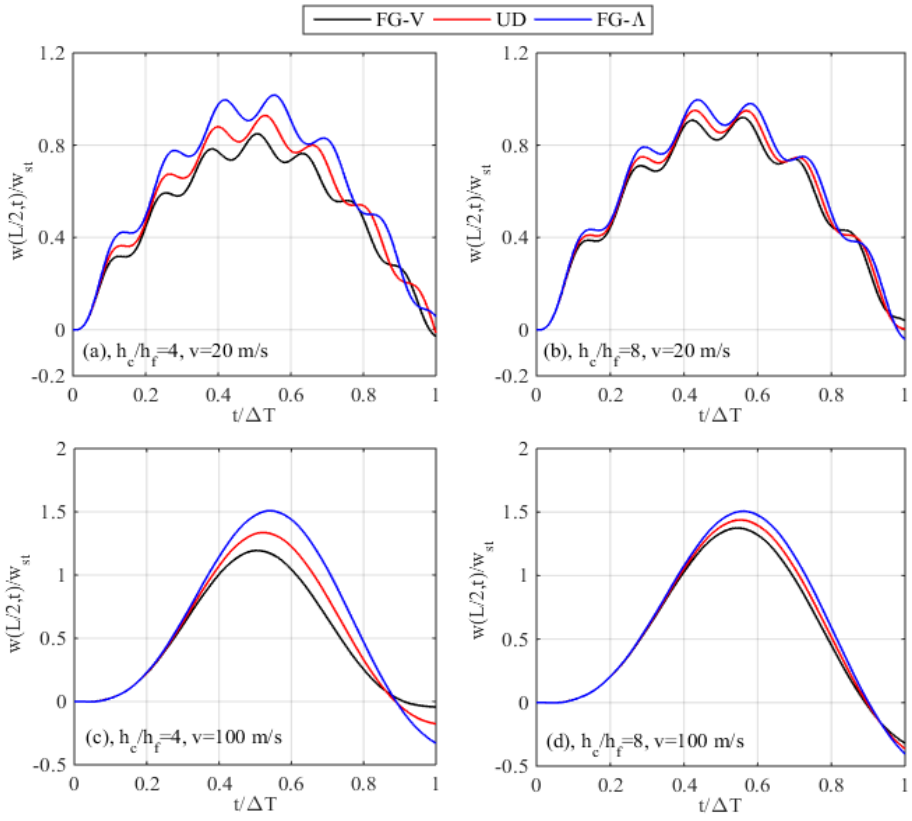

Figure 3. Time histories for dimensionless mid-span transverse displacement for different types of CNT distribution (*L/h* = 20, $V_{CNT}^{*} = 0.17$)

The difference of three types of CNT distribution is clearly seen from the figure, especially for the smaller values of h_c/h_f (Figure 3a, c). The mid-span deflection of the sandwich beams corresponding to the distribution FG-V of CNT is the smallest, while that of the sandwich beam with FG-Λ type distribution is the highest. For both values of the h_c/h_f ratio, the mid-span deflection increases with increasing moving load velocity. In addition, the sandwich beam is subjected to more vibration cycles when it is under load with lower moving velocities. This can be explained by the lower ratio of the moving load speed to the critical speed as in case of the isotropic beams [19]. As can be observed from Figure 3, the mid-span deflection of the FG-V beam insignificantly increases when increasing the h_c/h_f ratio, regardless of the moving velocity.

Table 6. Dynamic magnification factors for *L/h* = 20 and at different moving load velocities and h_c/h_f ratios

v (m/s)	Type	$h_c/h_f = 8$			$h_c/h_f = 6$			$h_c/h_f = 4$		
		V^*_{CNT}			V^*_{CNT}			V^*_{CNT}		
		0.12	0.17	0.28	0.12	0.17	0.28	0.12	0.17	0.28
20	UD	1.1778	0.9509	0.7275	1.1925	0.9419	0.6827	1.2102	0.9284	0.6216
	FG-X	1.1766	0.9496	0.7264	1.1900	0.9401	0.6808	1.2040	0.9241	0.6177
	FG-O	1.1790	0.9522	0.7284	1.1949	0.9436	0.6846	1.2162	0.9327	0.6256
	FG-V	1.1367	0.9198	0.6929	1.1285	0.8958	0.6345	1.0993	0.8492	0.5669
	FG-Λ	1.2213	0.9969	0.7643	1.2622	0.9916	0.7363	1.3396	1.0171	0.7070
50	UD	1.2070	0.9905	0.7892	1.2138	0.9913	0.7506	1.2162	0.9907	0.6965
	FG-X	1.2055	0.9898	0.7882	1.2107	0.9897	0.7487	1.2089	0.9868	0.6925
	FG-O	1.2085	0.9912	0.7901	1.2167	0.9928	0.7523	1.2234	0.9946	0.7005
	FG-V	1.1558	0.9649	0.7564	1.1357	0.9502	0.7036	1.1327	0.9173	0.6247
	FG-Λ	1.2621	1.0164	0.8239	1.3010	1.0335	0.8019	1.3753	1.0703	0.7810
100	UD	1.7810	1.4380	1.0152	1.8025	1.3967	0.9341	1.8286	1.3357	0.8311
	FG-X	1.7791	1.4361	1.0134	1.7987	1.3932	0.9311	1.8194	1.3278	0.8251
	FG-O	1.7828	1.4399	1.0168	1.8061	1.4002	0.9370	1.8378	1.3437	0.8370
	FG-V	1.7180	1.3743	0.9576	1.7053	1.3052	0.8587	1.6619	1.1938	0.7281
	FG-Λ	1.8479	1.5068	1.0785	1.9093	1.4996	1.0211	2.0258	1.5083	0.9611

Table 7. Dynamic magnification factors for *L/h* = 5 and at different moving load velocities and h_c/h_f ratios

v (m/s)	Type	$h_c/h_f = 8$			$h_c/h_f = 6$			$h_c/h_f = 4$		
		V^*_{CNT}			V^*_{CNT}			V^*_{CNT}		
		0.12	0.17	0.28	0.12	0.17	0.28	0.12	0.17	0.28
20	UD	1.2313	1.0400	0.8053	1.2506	1.0266	0.7675	1.2844	1.0090	0.7259
	FG-X	1.2297	1.0384	0.8036	1.2479	1.0239	0.7647	1.2775	1.0024	0.7205
	FG-O	1.2328	1.0416	0.8068	1.2533	1.0295	0.7700	1.2911	1.0159	0.7313

	FG-V	1.1933	1.0015	0.7680	1.1955	0.9721	0.7204	1.1842	0.9253	0.6593
	FG- Λ	1.2741	1.0839	0.8442	1.3166	1.0876	0.8097	1.3983	1.1137	0.8097
50	UD	1.2683	1.0724	0.8245	1.2914	1.0514	0.7873	1.3255	1.0224	0.7336
	FG-X	1.2669	1.0707	0.8229	1.2886	1.0481	0.7842	1.3183	1.0171	0.7274
	FG-O	1.2697	1.0741	0.8259	1.2940	1.0546	0.7902	1.3325	1.0276	0.7400
	FG-V	1.2323	1.0292	0.7887	1.2339	0.9871	0.7350	1.2215	0.9464	0.6731
	FG- Λ	1.3052	1.1180	0.8616	1.3514	1.1216	0.8438	1.4395	1.1408	0.8285
100	UD	1.2662	1.1049	0.8656	1.2923	1.0982	0.8178	1.3409	1.0884	0.7540
	FG-X	1.2644	1.1035	0.8638	1.2903	1.0955	0.8145	1.3356	1.0817	0.7472
	FG-O	1.2679	1.1063	0.8673	1.2944	1.1009	0.8209	1.3462	1.0951	0.7607
	FG-V	1.2338	1.0697	0.8238	1.2467	1.0446	0.7590	1.2568	0.9959	0.6741
	FG- Λ	1.3190	1.1416	0.9100	1.3599	1.1553	0.8830	1.4392	1.1908	0.8580

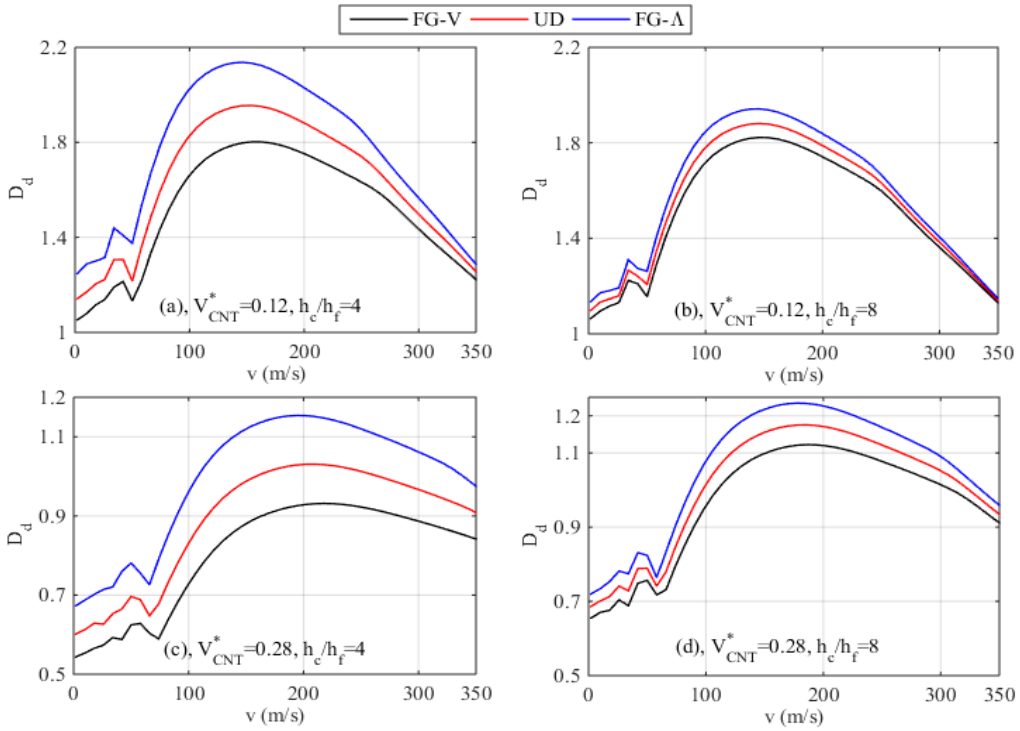

Figure 4. Variation of dynamic magnification factor with type of CNT distribution (*L/h*=20)

Tables 6-7 present the dynamic magnification factor D_d of FG-CNTRC sandwich beam for five different types of CNT distribution and different moving load velocities. The aspect ratios *L/h* = 20 and *L/h* = 5 are respectively used in the computation in two tables. It is observed from the tables that the factor D_d decreases with increasing the total CNTs volume fraction V_{CNT}^*, regardless of the CNT distribution. This decrease is observed more clearly when the moving load velocity is greater and the h_c/h_f ratio is smaller. Similar to the frequency parameter, the factor D_d obtained for three types of CNT distribution, UD, FG-X and FG-O, are

quite close together, while the factors D_d received from FG-V and FG-Λ distributions are the smallest and highest, respectively.

In the Figure 4, the relation between the dynamic magnification factor D_d and the moving load speed v is illustrated for FG-V, UD and FG-Λ sandwich beams. Two values of the total CNTs volume fraction $V_{CNT}^{*} = 0.12$, $V_{CNT}^{*} = 0.28$, and two values of the ratio $h_c/h_f = 4$ and $h_c/h_f = 8$ are chosen to plot the figure. Once again, we can see that when V_{CNT}^{*} is higher and the h_c/h_f ratio is smaller, the factor D_d received from the beams corresponding to the three types of CNT distribution is markedly different. Moreover, for the beams with $V_{CNT}^{*} = 0.28$, the factor D_d significantly increases with increasing the h_c/h_f ratio and this is clearly observed for all FG-V, UD and FG-Λ sandwich beams. Especially, the dynamic magnification factor D_d achieves the maximum value at a higher moving load speed for the beam having a lower h_c/h_f ratio and higher V_{CNT}^{*}.

6. CONCLUSIONS

Vibration of FG-CNTRC sandwich beams under a moving load with five different types of CNT distribution has been presented. The sandwich beam consists of three layers, a homogeneous core and two face sheets of CNTRC materials. The effective properties of two CNTRC faces are determined by the extended rule of mixture. Based on the third-order shear deformation theory, a finite element formulation has been derived and employed to investigate vibration characteristics of the beam. The obtained numerical results show that CNT distribution has an important influence on the vibration behavior of the beam. An increase of the total volume fraction of CNTs leads to an increase in the frequency parameter and a decrease in the dynamic magnification factor, and the effect of CNT volume fraction is more significant for the beam with a smaller h_c/h_f ratio. This study also shows that among the five types of the CNT distribution, the sandwich beam with FG-V type of CNT distribution has the lowest dynamic magnification factor while its fundamental frequency is the highest. Noting that although the numerical investigation presented here is only for simply supported beams, the formulation derived in the present work can also be used for FG-CNTRC sandwich beam analysis with other boundary conditions.

CRediT authorship contribution statement. Dr. Thi Thom Tran developed the computer code used in analysis and prepared the manuscript. Master Thi Hien Trinh performed the computations. Dr. Dinh Kien Nguyen set up the problem, checked the results and final manuscript.

Declaration of competing interest. We declare that we have no known competing financial interests or personal relationships that could have appeared to influence the work reported in this paper.

REFERENCES

1. Ke L. L., Yang J. and Kitipornchai S. - Nonlinear free vibration of functionally graded carbon nanotubereinforced composite beams, Compos. Struct. **92** (2010) 676-683.
2. Ke L. -L., Yang J. and Kitipornchai S. - Dynamic stability of functionally graded carbon nanotube reinforced composite beams, Mech. Adv. Mater. Struct. **20** (2013) 28-37.

3. Yas M. H. and Heshmati M. - Dynamic analysis of functionally graded nanocomposite beams reinforced by randomly oriented carbon nanotube under the action of moving load, Appl. Math. Model. **36** (2012) 1371- 94.
4. Yas M. H. and Samadi N. - Free vibrations and buckling analysis of carbon nanotube-reinforced composite Timoshenko beams on elastic foundation, Int. J. Pressure Vessels Pip. **98** (2012) 119-128.
5. Shen H. -S. and Xiang Y. - Nonlinear analysis of nanotube-reinforced composite beams resting on elastic foundations in thermal environments, Eng. Struct. **56** (2013) 698-708. doi:10.1016/j.engstruct.2013.06.002
6. Ansari R., Faghih Shojaei M., Mohammadi V., Gholami R. and Sadeghi F. - Nonlinear forced vibration analysis of functionally graded carbon nanotube-reinforced composite Timoshenko beams, Compos. Struct. **13** (2014) 316-327.
7. Lin F. and Xiang Y. - Vibration of carbon nanotube reinforced composite beams based on the first and third order beam theories, Appl. Math. Model. **38** (2014) 3741-3754.
8. Nejati M., Eslampanah A. and Najafizadeh M. - Buckling and Vibration Analysis of Functionally Graded Carbon Nanotube-Reinforced Beam Under Axial Load, Int. J. Appl. Mech. **8**(1) (2016) 1650008. https://doi.org/10.1142/S1758825116500083
9. Wu H. L., Yang J. and Kitipornchai S. - Nonlinear vibration of functionally graded carbon nanotube-reinforced composite beams with geometric imperfections, Compos. Part B: Eng. **90** (2016) 86-96.

   https://doi.org/https://doi.org/10.1016/j.compositesb.2015.12.007
10. Shafiei H. and Setoodeh A. R. - Nonlinear free vibration and post-buckling of FG-CNTRC beams on nonlinear foundation, Steel. Compos. Struct. **24** (2017) 65-77. https://doi.org/10.12989/scs.2017.24.1.065
11. Mohseni A. and Shakouri M. - Vibration and stability analysis of functionally graded CNT-reinforced composite beams with variable thickness on elastic foundation, Proc. IMechE. Part L: J. Materials: Design and Applications, **233**(2) (2019) 1-12.
12. Wu H. and Kitipornchai S. - Free vibration and buckling analysis of sandwich beams with functionally graded carbon nanotube-reinforced composite face sheets, Int. J. Struct. Stab. Dyn. **15**(7) (2015) 1540011. DOI: 10.1142/S0219455415400118
13. Ebrahimi F. and Farazmandnia N. - Thermo-mechanical vibration analysis of sandwich beams with functionally graded carbon nanotube-reinforced composite face sheets based on a higher-order shear deformation beam theory, Mech. Adv. Mater. Struct. **24** (2017). https://doi.org/10.1080/15376494.2016.1196786
14. Nguyen D.K., Nguyen Q.H., Tran T.T. and Bui V.T. - Vibration of bi-directional functionally graded Timoshenko beams excited by a moving load, Acta Mech. **228** (2017) 141-155.
15. Vu T.A.N, Le T.N.A. and Nguyen D.K. - Vibration of two-directional functionally graded sandwich beams traversed by a harmonic load, Vietnam J. Sci. Tech. **58**(6) (2020) 760-775.
16. Shi G. - A new simple third-order shear deformation theory of plates, Int. J. Solids Struct. **44** (2007) 4399-417.

17. Shi G., Lam K. Y. and Tay T. E. - On efficient finite element modeling of composite beams and plates using higher-order theories and an accurate composite beam element, Compos. Struct. **41** (1998) 159-165.
18. Han Y. and Elliott J. - Molecular dynamics simulations of the elastic properties of polymer/carbon nanotube composites, Comp. Mater. Sci. **39**(2) (2007) 315–323.
19. Olsson M. - On the fundamental moving load problem, J. Sound Vib. **145** (1991) 229-307.